IEEE P802.15
Wireless Personal Area Networks

Project	IEEE P802.15 Working Group for Wireless Personal Area Networks (WPANs)
Title	**The Ultra-Wideband Indoor Multipath Model**
Date Submitted	July 8, 2002

Source		
	Dr. Saeed S. Ghassemzadeh AT&T Labs-Research Rm. B237, 180 Park Ave. Florham park, NJ 07932	Voice: 973-236-6793 Fax: 973-360-5877 E-mail: saeedg@research.att.com
	Dr. Larry J. Greenstein WINLAB-Rutgers University 73 Brett Road Piscataway, NJ 08854	Voice: 732-445-4992 Fax: 732-445-3693 E-mail: ljg@winlab.rutgers.edu
	Prof. Vahid Tarokh Division of Engineering & Applied Sciences Harvard University 33 Oxford Street Room MD 131 Cambridge, MA 02138	Voice: 617-384-5026 Fax: 617-496-6404 E-mail: vahid@deas.harvard.edu

Re:	IEEE P802.15-02/208r1-SG3a and IEEE P802.15-02/282r0-SG3a
Abstract	This contribution describes a simple model for simulation of the UWB indoor channel. It also consists of detailed characterization of channel parameters such as Doppler spectrum, maximum excess delay, mean and RMS delay spread, average multipath intensity profile, relative multipath powers and their amplitude and phase distribution. This work is based on over 300,000 UWB frequency response measurements at 712 locations in 23 homes.
Purpose	For IEEE 802.15.SG3a to adopt the multipath profile model and the associated channel parameters and to use them for performance evaluation of various UWB PHY proposals.
Notice	This document has been prepared to assist the IEEE P802.15. It is offered as a basis for discussion and is not binding on the contributing individual(s) or organization(s). The material in this document is subject to change in form and content after further study. The contributor(s) reserve(s) the right to add, amend or withdraw material contained herein.
Release	The contributors acknowledge and accept that this contribution becomes the property of IEEE and may be made publicly available by P802.15.

Introduction

In general, many models are available in the literature for predictions and simulation of indoor channel. However, these models do not represent a UWB channel, or are not in the environment and/or frequency spectrum of interest, or have database that is too small for statistical characterization of the channel. This motivated us to perform extensive measurements in indoor environments, and to create a channel model for indoor UWB channels that:

- Provides a realistic UWB propagation channel without requiring costly sounding experiments
- Provides a compact and simple method for simulating the multipath channel behavior
- Is useable for performance evaluation of various PHYs in the in-home environment

Regression analyses of our extensive database have led us to a novel statistical characterization of the dB-power as a function of excess delay for the indoor UWB multipath channel. Our model statistically regenerates the statistics of the original data and replicates all statistical parameters of the indoor channel with small error. The result is a general statistical multipath model that is simple, accurate and can be upgraded with further measurements.

In Section 1, we give some theoretical background. Section 2 describes the data collection method, experiment setup and data reductions. Section 3 summarizes our key findings. Section 4, presents our model and is followed by conclusions and references.

1. Theory

The locations of ceilings, walls, doors, furniture and people inside a house result in the transmit signal taking multiple paths to the receiver. Hence, signals arrive at the receiver with different amplitudes, phases and delays. This phenomenon can be represented mathematically as:

$$h(t,\tau;d) = \sum_{i=1}^{L} a_i(t,d)\exp(j\theta_i(t,d))\delta(t-\tau_i) \qquad (1)$$

which represents the complex impulse response of the channel. In equation (1), d denotes the T-R separation, L is the number of multipath components, α_i represents the amplitude of the i^{th} multipath component, θ_i is the phase associated with the i^{th} path, τ_i is the time delay of the i^{th} path in the channel with respect to the first arriving multipath and δ is the Dirac delta function. We refer to the impulse response as the Multipath Intensity Profile (MIP) when the eq.(1) is appropriately normalized to its average total power (i.e., With the average path gain information removed from data. We also refer to "relative MIPs" as the MIPs that are normalized to their maximum return power. We base part of the multipath channel characterization on RMS delay spread τ_{RMS}, which is a measure of multipath spread within the channel. It is an important

parameter for characterizing time dispersion or frequency selectivity. It is the square root of the second central moment of the power delay profile and is given by

$$\tau_{RMS} = \sqrt{\sum_{i=1}^{L} (\tau_i - \tau_m)^2 \left|h(t,\tau_i)\right|^2}$$
$$\tau_m = \sum_{i=1}^{L} \tau_i \cdot \left|h(t,\tau_i)\right|^2 \qquad (2)$$

Here τ_m is the mean excess delay (the first moment of the MIP), and we assume that *h*'s are scaled such that their squared magnitude sum to 1. Although large delay spreads occur rarely, they can have a major impact on system performance. To accurately evaluate a candidate UWB system proposal, it is desirable to model the variability of the delay spread in worst-case scenarios.

Tapped-delay line model is the starting point of our impulse response channel modeling. This type of model generally is characterized by the number of taps, the time delay relative to the first tap (i.e., τ_0 = 0 ns), the average power relative to the strongest tap and the Doppler spectrum of each tap. With a single tapped-delay line, we cannot capture the delay spread variability. We, therefore, propose a statistical model to generate the parameters of the tapped-delay line. The model will generate a relative MIP. Let P_r represent the relative power of a multipath component with respect to the maximum return. Then the average total power P_{ave} is:

$$P_{\text{ave}} = \sum_{i=0}^{L-1} P_{ri} \qquad (3)$$

Given *L* dB path loss at so many meters then the average power of the individual multipath component is:

$$P_i = \frac{LP_{ri}}{P_{\text{ave}}} \qquad (4)$$

This multipath component average power appropriately scales the transmitted signal to its average level. At this point, knowing the relative delay along with amplitude and phase distribution of the multipath components would give complete knowledge o the channel.

2. Measurements: Equipment, Experiment setup and Data Reduction

2.1. Channel Sounding Equipment

Figure 1 illustrates the transceiver configurations. A Vector Network Analyzer (VNA) is used for measuring the frequency response of the channel. The VNA generates a signal as the input to a variable attenuator and a 34-dB gain broadband transmitter/RF amplifier chain. The output of the RF power amplifier is propagated by a vertically polarized, conical monopole, omni-directional (in the H-plane) over the 4.375 – 5.625 GHz frequency range. The signal from the identical conical monopole receive antenna is first passed through a Low Noise Amplifier (LNA) with a gain of 34 dB. It is then returned to the VNA via 150 feet of coaxial cable with a 17-dB loss followed by another LNA with a gain of 36 dB. High quality doubly-shielded cable was used to insure no leakage from the air into the receiver by the cable. The VNA records the variation of 401 complex tones across the above-mentioned frequency range. The VNA sweeps the frequency range for 401 received tones and compares them to pre-calibrated coefficients. The sweep rate for all tones is slightly over 400 ms corresponding to a maximum measurable Doppler spread of about 2.5 Hz. Programs in HP VEE software were written to control the VNA measurement system. The complex data from the VNA was stored on a laptop computer via a GP-IB interface.

2.2. Experiment Setup

Using the techniques and hardware mentioned above, experiments were performed inside 23 homes in the northern and central New Jersey. The homes had differing structure, age, size and clutter. The transmit antenna from the VNA was always located in a fixed position, and the dual receiving antenna mast was moved throughout each house on a pre-measured grid. Knowledge of the physical distance between the transmitter and receiver allowed the measured data to be correlated with the distance. For all measurements, the heights of both the transmit and receive antennas were fixed at 1.8 m (6-feet). Figure 2 illustrates a typical home layout and measurement setup.

Measurements were made while the transimt/receive antennas were within Line-of-Sight (LOS) of each other and while they were within non-LOS (NLS) of each other. Two different experiments were performed in each home. In 15 homes, we selected over 20 LOS locations and over 20 NLS locations. We then measured the channel frequency response observed from each of two antennas separated by 38 inches, simultaneously, over a 1.8-minute period (273 snapshots). In the remaining eight homes, we used only one receive antenna, 10 LOS and 10 NLS locations. Hence, our database contains about 1240×273 measurements of the channel frequency response. The transmit antenna location was placed for best signal coverage inside each home and optimized for minimum possible T-R separation for NLS experiments. The transmitter's power level was adjusted so that the VNA always operated within the linear range

of its detectors and well above noise floor. All measurements were performed on the same floor of each home so that variations in the pattern of the receiving and transmitting antenna did not have to be taken into account.

2.3. Data Reduction

The set of measured data was preprocessed to make it proper for our analysis. The main issues in preprocessing are the removal of calibration data from the measured data, data normalization, setting a threshold for the noise floor and the synchronization of all profiles to a point in time (i.e., by τ_0 we refer to the first multipath arrival time above the noise floor.). Of course, τ_0 had to be carefully selected so that there is no ambiguity in its presence. In this section we explain exactly how all of these were performed without injecting any introducing new impurities into data itself. Specifically, we used the following steps for data reduction.:

- All calibration information is removed from the raw data. This step insures that all the hardware impurities are removed from the data so that the results only reflect the changes due to propagation channel only.
- The response is then locally averaged over time (since the receiver was kept stationary and maximum Doppler measured was no more than a few tenths of Hz.).
- We then performed, 401-point complex IFFT on each frequency response profile to get the complex impulse response profile.
- The Impulse responses are then normalized to the total average power.
- We set a threshold (-30 dB or 0.001) of 10 dB above the average noise floor (-40 dB). All returns below this threshold were set to this threshold (i.e. 0.001 or –30 dB).
- We then subtracted the noise from the profiles so that the impulse response noise floor is equivalently zero. The new profile is then re-normalized so that the total power in each profile is one. We refer to this profile as Multipath Intensity Profile (MIP). Note that this step would decrease the average power by 3%. However, we could not avoid this since many points existed at noise floor following the maximum excess delay. Keeping these points in profiles would have complicated the model.
- We then aligned all profiles such that their delays at zero ns represent the first return above the threshold.
- Lastly, the LOS data was separated from the NLS.

3. Key findings

Over 300,000 MIPs were collected and analyzed. The key findings are as follows:

- For the LOS data, the relative MIPs include a strong return at τ_0 followed by a sharp drop and then a more-or-less exponential decrease on a linear τ-scale. This suggests that a model for LOS profiles consisting of a Kroneker delta function at $\tau = 0$, plus a linear decrease in dB-power with τ.
- On the average, the first few returns (i.e., The return at $\tau_0 = 0$ ns) of the MIP is not always the strongest return in NLS profiles and have lower average power with respect to the maximum return.
- The relative MIPs are best described by a few weak returns followed by maximum return and then a short drop followed by an exponential decrease on a linear scale. This indicates that a good model should account for this type of channel behavior.
- While the average relative power of each multipath while
- The values of τ_m and τ_{RMS} are normally (i.e., Gauss-) distributed over all homes, with mean values of 4.7 ns and 8.5 ns and standard deviation values of 2.3 ns and 3.5 ns, in LOS and NLS, respectively.
- τ_{RMS} increases as $d^{0.27}$ and $d^{0.4}$ for LOS and NLOS, respectively.
- The mean τ_{RMS} and mean path loss were obtained by averaging over 273 profiles for each location at each home. A comparison of their values over 23 homes indicates an increase in τ_{RMS} with increasing path loss. This anticipated increase in τ_{RMS} is largely due to the paths with longer delays having larger path loss values associated with them.
- No significant excess delays above 70 ns were observed for a 30 dB threshold.
- τ_{RMS} values were compared as a function of dB threshold level (i.e., -5, -10, -15, -20 and -30) relative to below the maximum return in the average relative MIP. A summary of these values is given in Table I and II. The results showed that the mean excess delay and RMS delay spread increases with decreasing threshold, as expected. Furthermore, These observations are consistent with some frequency domain measurements reported in the literature.
- The maximum significant Doppler frequency observed was 0.1 Hz.
- The multipath amplitudes undergo small variation that can be best characterized by Rician distribution with a K-factor greater than 40 dB.
- The phases of the multipath components are uniformly distributed between 0 and 2π.
- The multipath components are correlated with correlation coefficient $0 \leq \rho \leq \sim 0.3$, with ρ generally decreasing with increasing path delay separation.

4. The Channel Impulse Response Model

Our approach is to use the relative MIP, defined as follows: There is an average, over all the locations of a given home, of the (unit-area) delay profile. At some delay, the average return is a maximum, and the value of this maximum average return can be identified. If each return at each location is normalized by this value, then the MIP at each location is said to be a relative MIP. (The average return at the maximizing delay will, by definition, be 1.) We describe a simple statistical model for generating the relative MIP at any location in any home, which can then be used to generate a unit-area delay profile and—from that—a complex impulse response.

4.1. The LOS Multipath Channel Model

We recall that, in LOS environment, the relative MIPs contain a strong return at τ_0 followed by a sharp drop (See Figure 8.) and then a more-or-less exponential decrease on a linear τ-scale. This suggests a model for LOS profiles consisting of a Kroneker delta function at $\tau = 0$, plus a linear decrease in dB-power with τ. This function can be represented as:

$$P|_{\text{linear}} = \delta(\tau) + \widetilde{S}\widetilde{C}e^{\widetilde{\alpha}\tau}u(\tau - \tau_1) \tag{5}$$

or on a dB-scale:

$$P|_{\text{dB}} = \begin{cases} 0 & \text{for} \quad \tau = 0 \\ (C + \alpha\tau + S)\,u\,(\tau - 0.8ns) & \text{for} \quad \tau > 0 \end{cases} \tag{6}$$

C is the intercept value, and, α is the slope of the line that fits the average relative MIP in each home. C and α are chosen such that the mean-square value of the dB variation, S, is minimized. We have characterized these parameters over our database. We found to a good approximation, that:

- *C* is a normally distributed r.v., N[-6.38, 1.98] dB. See Figure 9.
- α is normally distributed r.v. N[-0.82, 0.25] dB. See Figure 9.
- S in dB is a normally distributed r.v. over delay, different from location to location within the same home but having the same mean and standard deviation. See Figure 10.
- Mean of S is fairly constant over all homes (-0.41), while its standard deviation is a normally distributed r.v., N[6.86, 0.923]. See Figure 10.

Based on these results, we introduce four random variates as follows:

$$\alpha = \mu_\alpha + n_1\sigma_\alpha,\ C = \mu_c + n_2\sigma_c,\ S = \mu_s + n_3\sigma_s, \sigma_s = \mu_\sigma + n_4\sigma_\sigma \tag{7}$$

Inserting (7) into (6): and we have:

$$\begin{aligned}\overline{P_{rel}(\tau)}\Big|_{\text{dB}} &= \left[\mu_c + \tau\mu_\alpha + \mu_s\right]u\left(\tau - 0.8ns\right) \\ &+\left[n_2\sigma_c + n_1\sigma_\alpha\tau + n_3\mu_\sigma + n_3n_4\sigma_\sigma\right]u\left(\tau - 0.8ns\right) \qquad d_o \le d \le 15 \text{ m } \&\ \tau \ge 0\end{aligned} \tag{8}$$

where n_1,n_2, n_3 and n_4 are i.i.d zero mean, unit variance Gaussian random variates. Since S varies from one delay to another then n_3 is a fast-varying quantity. Conversely, n_1, n_2 and n_3 are slow-varying quantities that change from one home to another.

The second bracketed term in (8) is the variable part of above equation is not precisely Gaussian, since $n_3 \times n_4$ is not Gaussian. However, this product is small with respect to the other three Gaussian terms. Finally, the relationships among the parameters in (5) and (6) are:

$$\begin{aligned} C &= 10\log_{10}\widetilde{C} \\ \alpha &= 10\widetilde{\alpha}\log_{10} C \\ S &= 10\log_{10}\widetilde{S} \end{aligned} \tag{9}$$

4.2. The NLS Multipath Channel Model

In NLS environments, we observed almost the same behavior as LOS environment with the exception that the first few returns that were blocked and therefore, were weaker than the maximum return having larger delay (See Figure 4.). Typically, however, representation of the MIPs in NLS environments has been reported as a decaying exponential. Following this intuition once again, we formed the following function:

$$P_{rel}(\tau)\Big|_{\text{dB}} = \alpha\tau + S \tag{10}$$

or in linear form:

$$P_{rel}(\tau)\Big|_{\text{linear}} = \widetilde{S}e^{\widetilde{\alpha}\tau} \tag{11}$$

where α is the decibel-decay constant and S is the dB variation about the mean relative MIP. The model assumes that the power of the first averaged return of the MIP is the strongest one. This

simplifies the model considerably, with insignificant change in the slope. The constant α is then found such that the mean-square value of the dB variation, S, is minimized. We then characterize α and S over the population of homes. We found to a good approximation, that:

- Value of α [dB/ns] is normally distributed r.v., N[-0.50, 0.13]. See Figure 5.
- *S* [dB] is a normally distributed r.v., over delay, different from location to location within the same home but having the same mean and standard deviation. See Figure 7.
- The mean of S is fairly constant over all homes (-0.41 dB), while its standard deviation is a normally distributed r.v., N[7.20, 0.88]. See Figure 6.

Based on these results, we introduce three random variables, as follows:

$$\alpha = \mu_\alpha + n_1\sigma_\alpha,\ S = \mu_s + n_2\sigma_s, \sigma_s = \mu_\sigma + n_3\sigma_\sigma \tag{12}$$

Inserting (12) in (10) and rearranging, we get:

$$\begin{aligned}\overline{P_{rel}(\tau)}\Big|_{\text{dB}} &= \left[\tau\mu_\alpha + \mu_s\right]u\left(\tau - 0.8ns\right) \\ &+ \left[n_1\sigma_\alpha\tau + n_2\mu_\sigma + n_2n_3\sigma_\sigma)\right]u\left(\tau - 0.8ns\right) \qquad \text{for } d_o \le d \le 15 \text{ m } \&\ \tau \ge 0\end{aligned} \tag{13}$$

Note again that n_1, n_2, and n_3 are iid zero-mean, unit-variance Gaussian variates. n_2 is a fast-varying quantity that changes from one delay to another, and n_1 and n_3 are slow-varying quantities that change from one home to another.

4.3. Simulation Results

Figure 8 shows the flowchart of a channel simulator that uses the above model to generate relative MIPs and, from that, produces the complex impulse responses that can be used in system simulations Using this flowchart, we simulated the model to compare its statistical behavior with that of measured data. Specifically, we looked at:

- CDFs of RMS delay spread: Simulated vs. measured. See Figure 12.
- Average MIP: Simulated vs. measured. See Figure 13
- CDF of the dB variations about the average: Simulated vs. measured. See Figure 14.

Conclusion

We have presented a simple statistical multipath model that is easily integrated with the path loss model. The model is based on over 300,000 UWB frequency responses at 712 locations in 23

homes. The model regenerates the statistical properties of the indoor channel with high accuracy. This model can be used for simulation and performance evaluation of any UWB system, and it can be upgraded with further measurements.

References

[1] K. Pahlavan, A.H. Levesque, Wireless Information Networks, John Wiley and Sons, New York, 1995.

[2] T.S. Rappaport, Wireless Communications, Principles and Practice, Prentice-Hall, New Jersey, 1996.

[3] A.A. Saleh, R.A. Valenzuela, "A Statistical Model For Indoor Multipath Propagation", IEEE J. Select. Areas Commun., 5:128-137, Feb. 1987.

[4] R.J.C. Bultitude, S.A. Mahmoud, W.A. Sullivan, "A Comparison of indoor radio propagation characteristics at 910 MHz and 1.75 GHz", IEEE J. Select. Areas Commun., 7:20-30, Jan 1989.

[5] T.S. Rappaport, S.Y. Seidel, K. Takamizawa, "Statistical Channel Impulse Response Models for Factory and Open Plan Building Radio Communication System Design", IEEE Trans. on Commun., 39:794-806, May 1991.

[6] S.S. Ghassemzadeh, V. Erceg, D.L. Schilling, M. Taylor, H. Arshad, "Indoor Propagation and Fading Characterization of Spread Spectrum Signal at 2 GHz", IEEE Globecom, 92.

[7] S.S. Ghassemzadeh, D.L. Schilling, Z. Hadad, "On the Statistics of Multipath Fading Using a Direct Sequence CDMA signal at 2 GHz", International Journal on Wireless Information Networks, April 1994.

[8] L. J. Greenstein, V. Erceg, Y. S. Yeh, and M. V. Clark, "A New Path-Gain/Delay-Spread Propagation Model for Digital Cellular Channels", IEEE Transaction on Vehic. Technology, 46:477-484, July 1999.

[9] S.J. Howard, K. Pahlavan, " Measurement and Analysis of the indoor radio channel in the frequency domain", IEEE Trans. Instrum. Measure., 39:751-755, Oct. 1990.

[10] S.J. Howard, K. Pahlavan, "Autoregressive Modeling of Wide-Band Indoor Radio Propagation", IEEE Transaction on Commun., 40:1540-1552, September 1992.

[11] H. Hashemi, "The indoor Propagation Channel", Proc. of the IEEE, 81:943-968, July, 1993

[12] M.Z. Win, R.A. Scholtz, M.A. Barnes, "Ultra-Wide Bandwidth Signal Propagation For Indoor Wireless Communications", Proc. of IEEE Int. Conf. Commun., 1:56-60, June 1997.

[13] D. Cassioli. A. Molisch, M.Z. Win, “A Statistical Model for UWB Indoor Channel”, Proc. of the IEEE VTC Spring 2001, 2001 Rhodes.

[15] R. Addler, D. Cheung, E. Green, M. Ho, Q. Li. C. Prettie, L. Rusch, K. Tinsley, “UWB Channel Measurements for the Home Environment”, UWB Intel Forum, 2001 Oregon.

[16] S.S. Ghassemzadeh, et.al. “A Statistical Path Loss Model for In-Home UWB Channels”, Proc. of the IEEE Conference on UWB Systems and technologies, May 2002 Baltimore.

[17] V. Erceg, D.G. Michelson, S.S. Ghassemadeh, et. al. "A Model for the Multipath Delay Profile of Fixed Wireless Channels", IEEE Journal on Selected Areas in Communications, March 1999

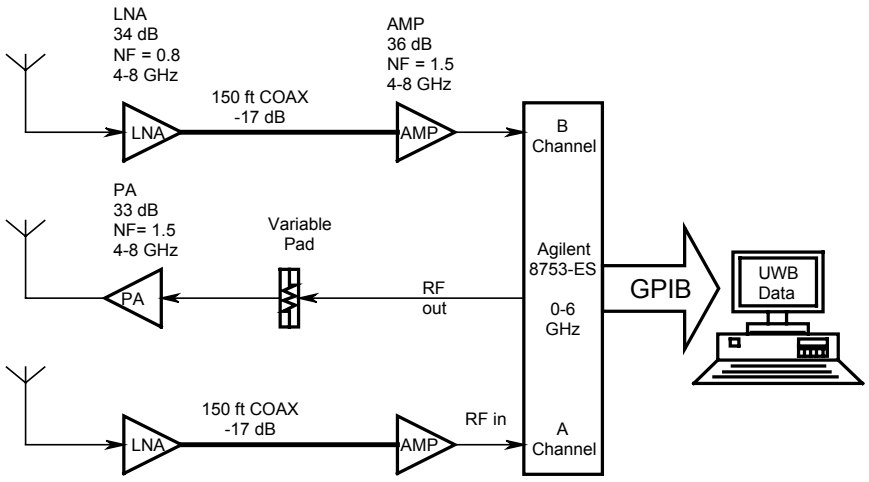

Figure 1: Channel Sounder Transceiver

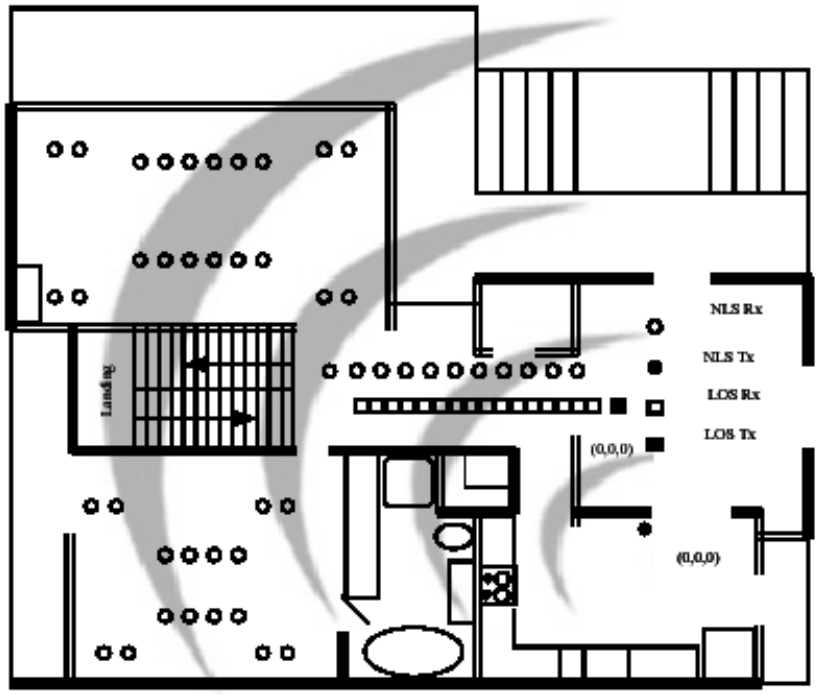

Figure 2: Typical home layout and measurement setup

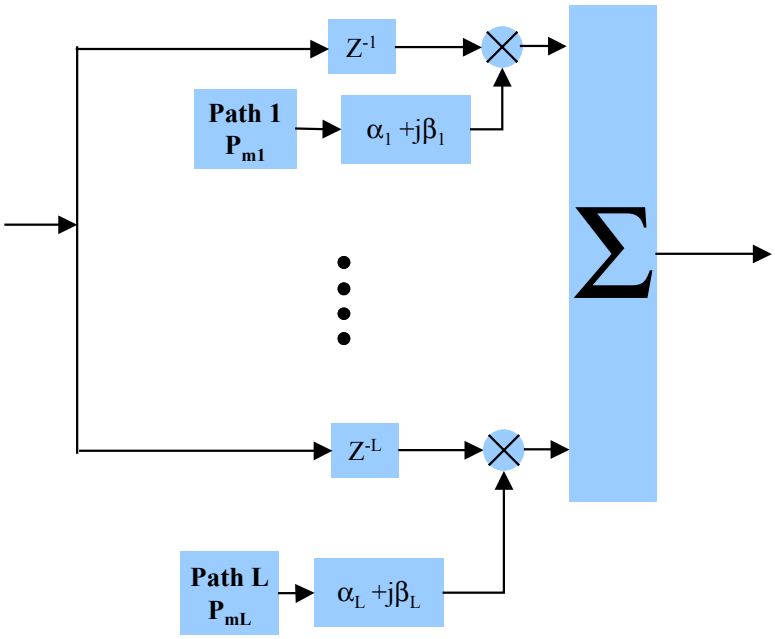

Figure 3: The tapped-delay line structure

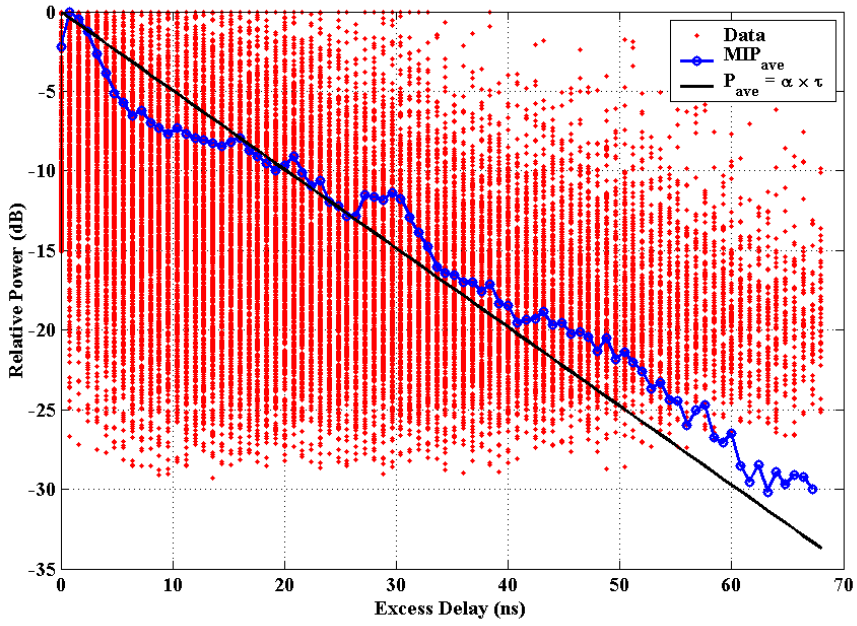

Figure 4: The relative MIP model in NLS environments

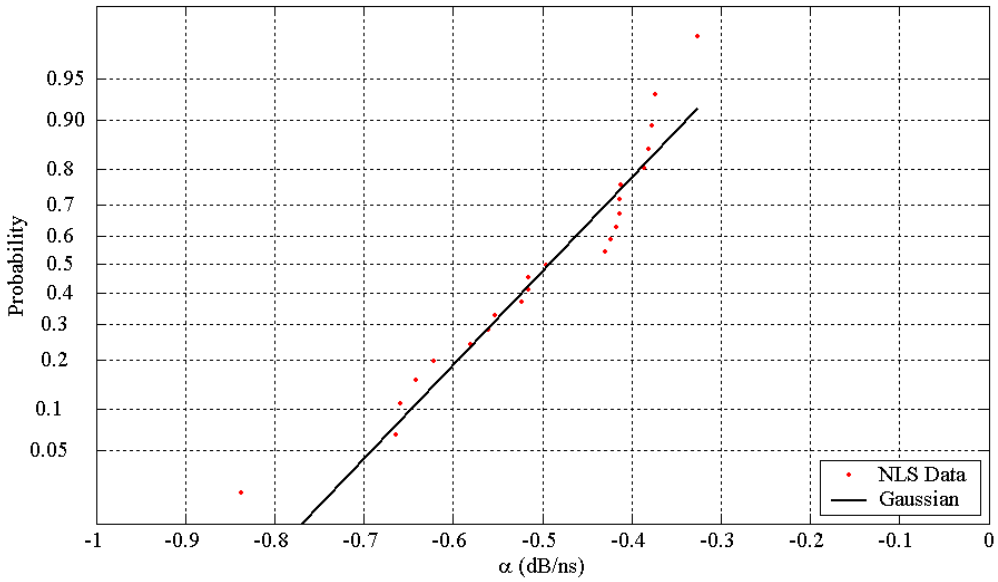

Figure 5: Distribution of α in NLS environments

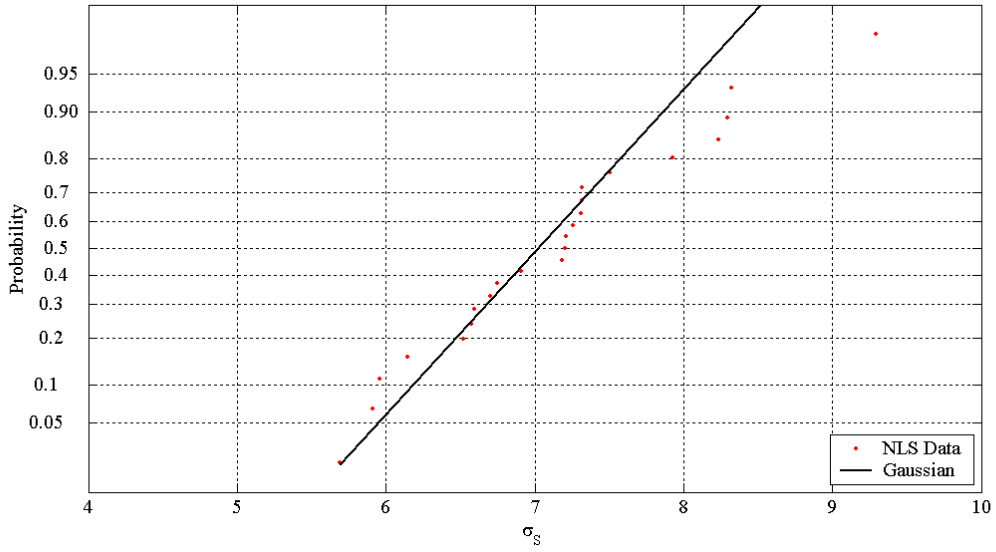

Figure 6: Distribution of σ_s in NLS environments

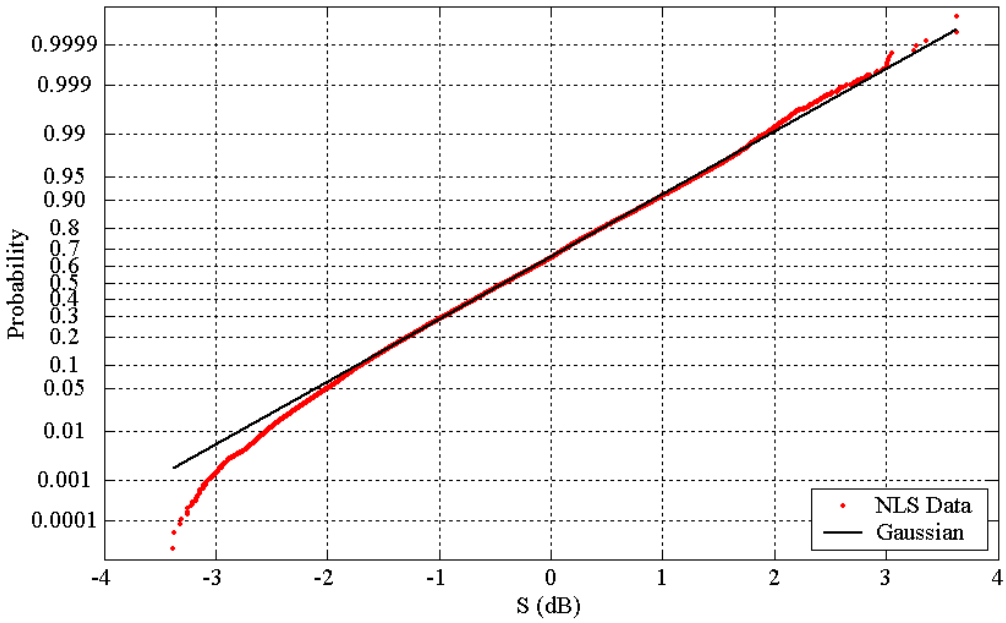

Figure 7: Distribution of S in NLS environments

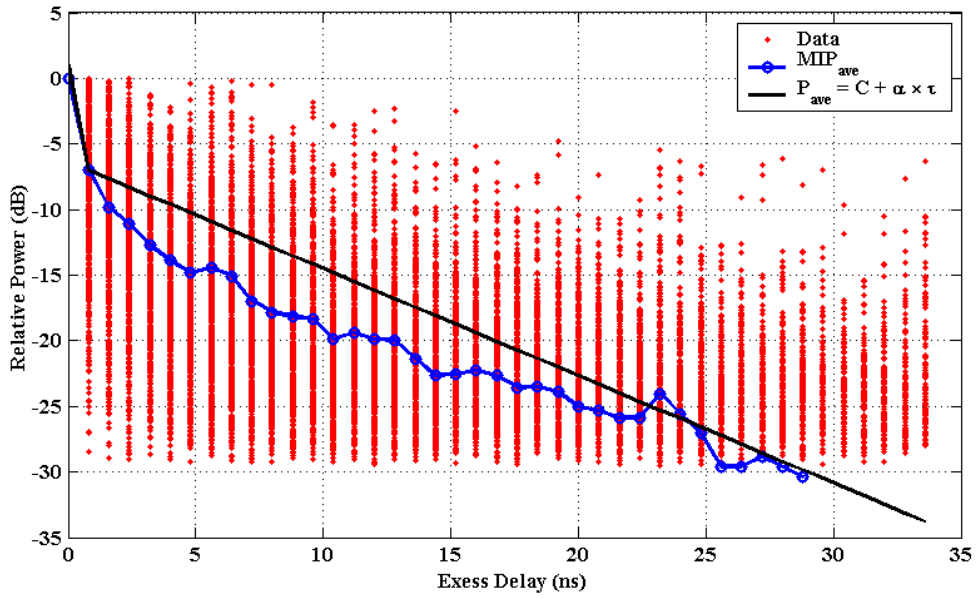

Figure 8: The relative MIP model in LOS environments

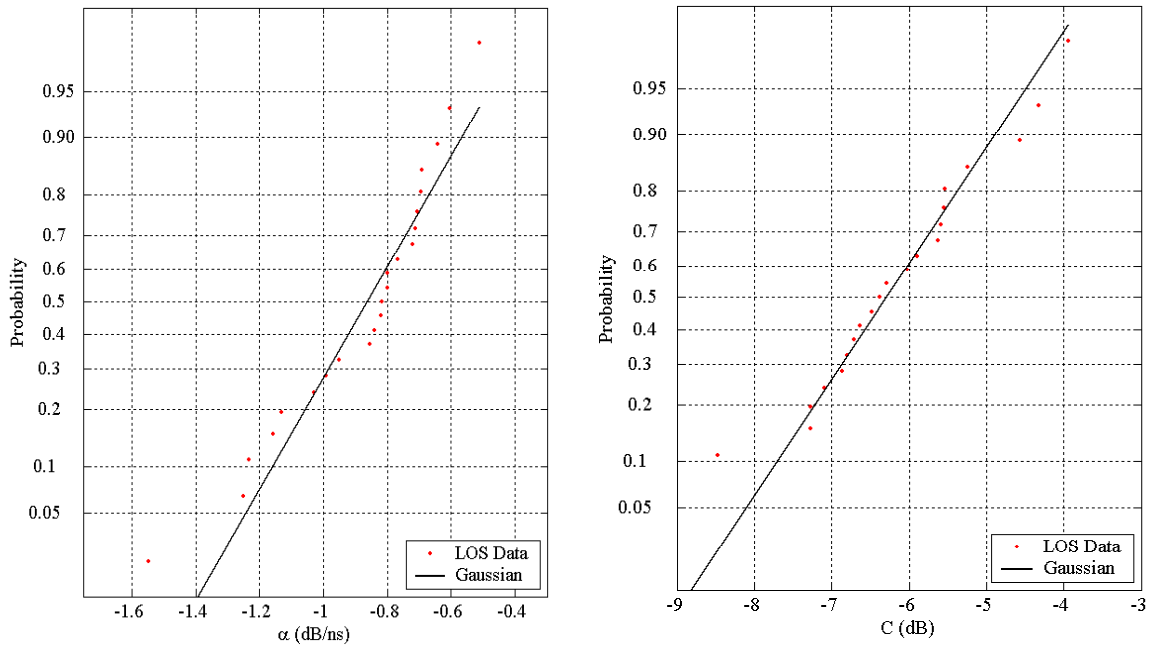

Figure 9: Distributions of C and α in LOS environments

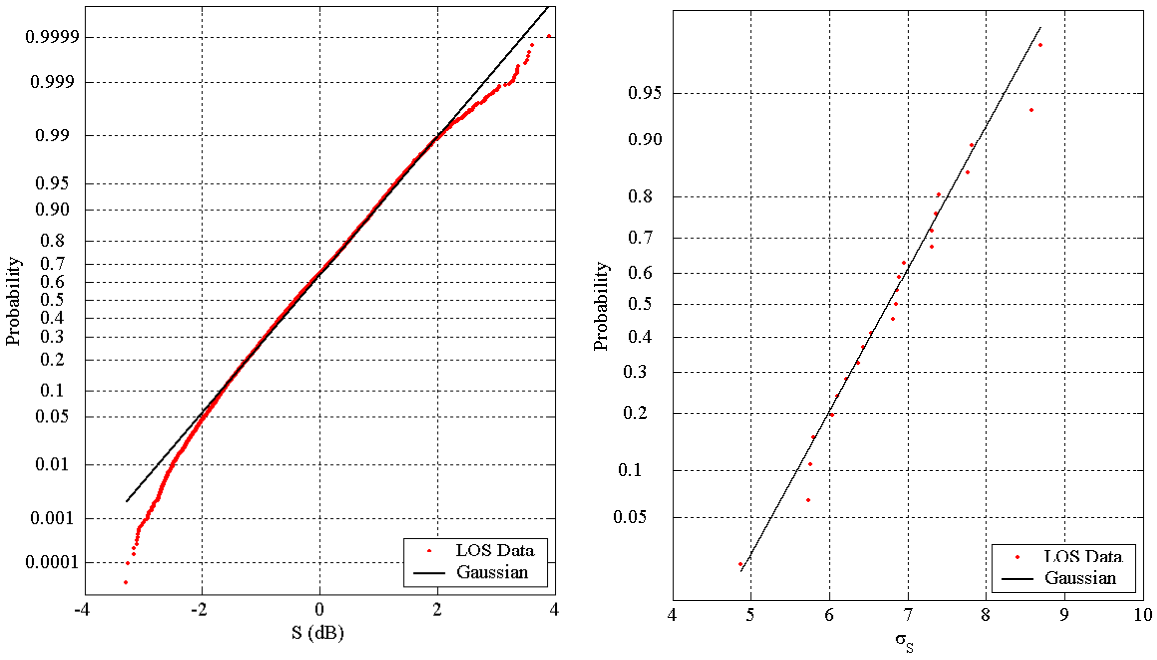

Figure 10: Distributions of S and σ_s in LOS environments

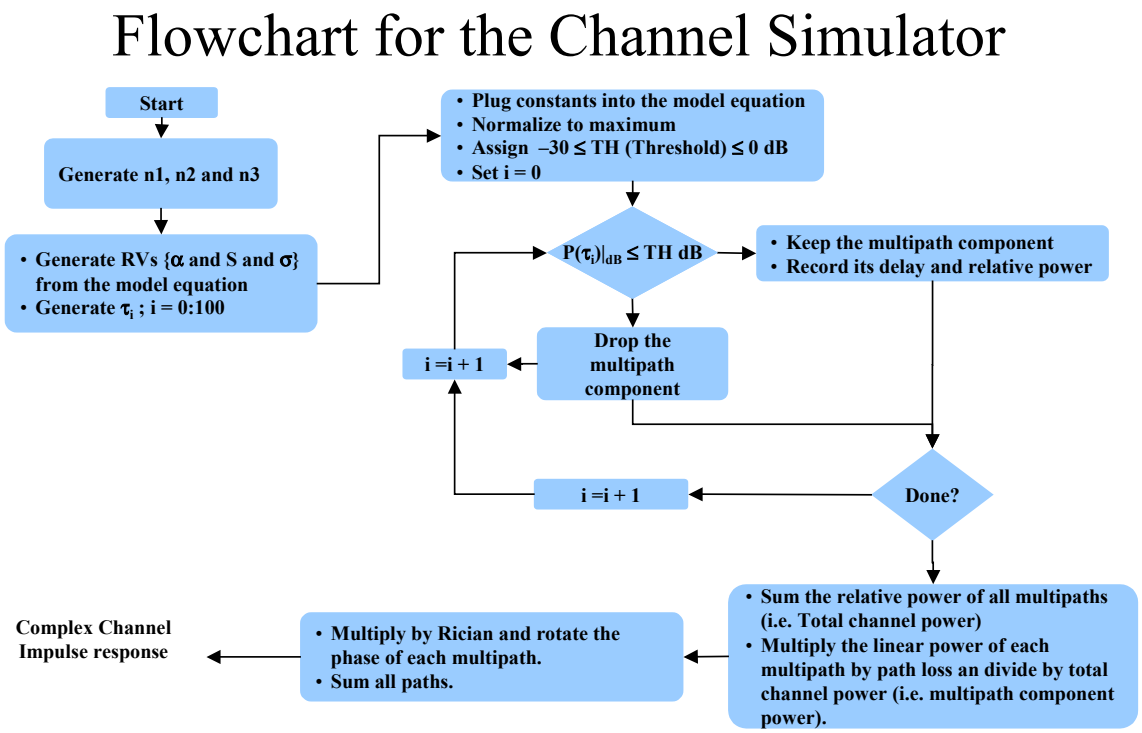

Figure 11: Flowchart of the UWB channel simulator

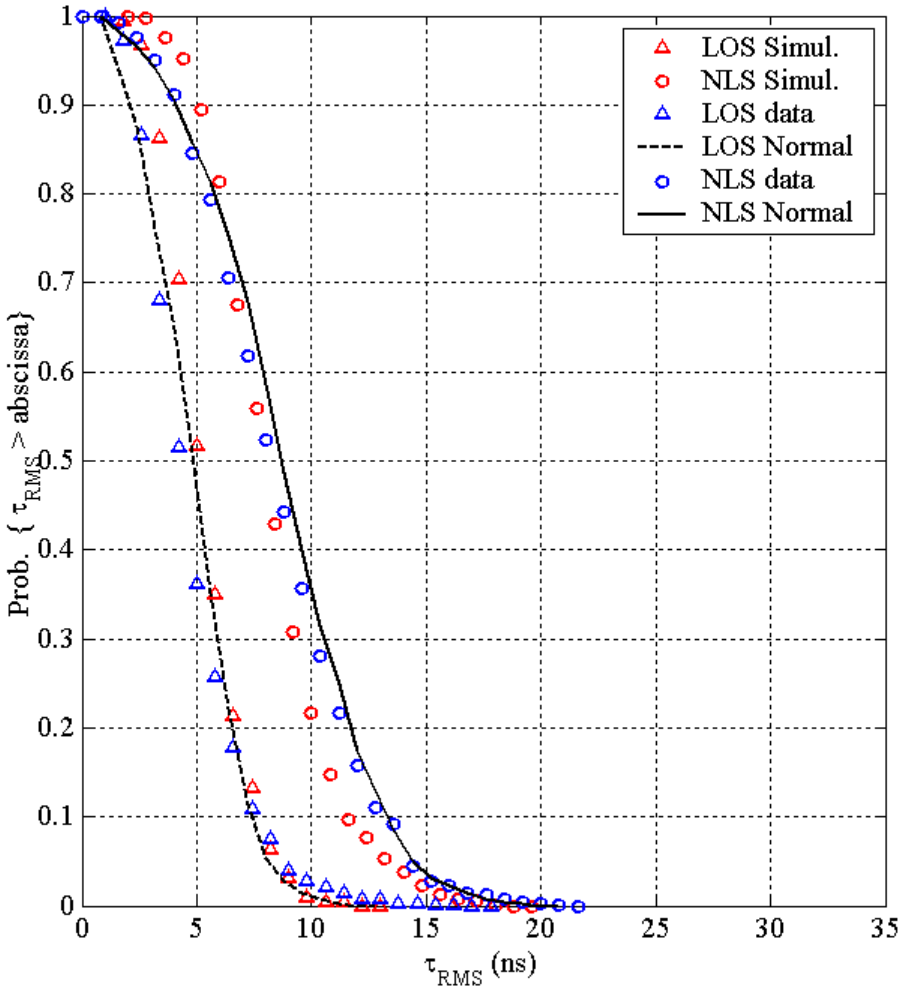

Figure 12: CDFs of RMS Delay Spread: Simulated vs. Measured

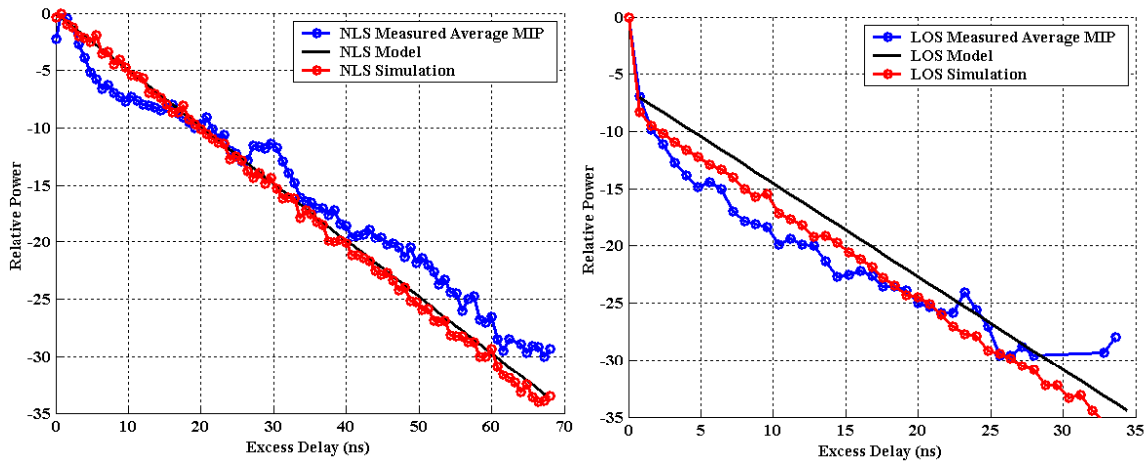

Figure 13: Average MIPs: Simulated vs. Measured

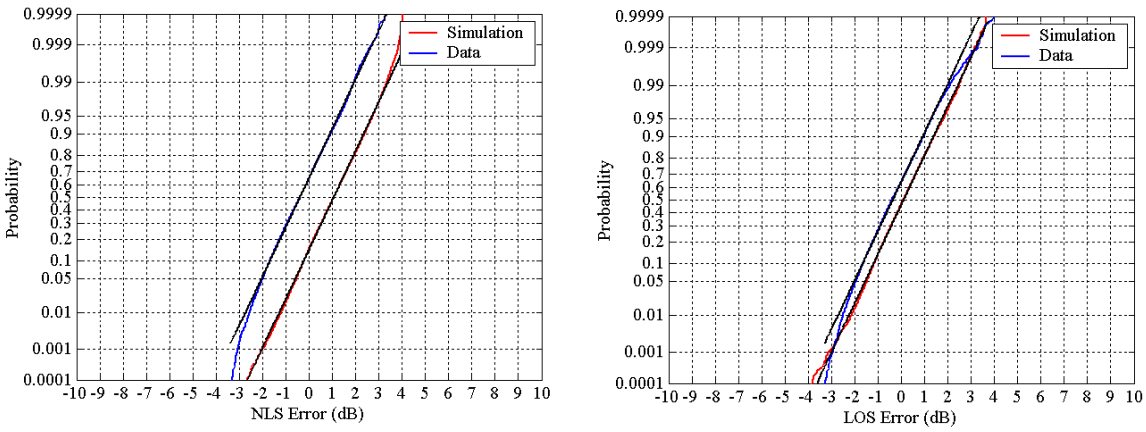

Figure 14: Model Errors: Simulated vs. Measured